Simulation Model of Reactive Nitrogen Species in an Urban Atmosphere using a Deep Neural Network: RNDv1.0

Junsu Gil[1], Meehye Lee[1*], Jeonghwan Kim[2], Gangwoong Lee[2], Joonyoung Ahn[3], Cheol-hee Kim[4]

[1] *Department of Earth and Environmental Sciences, Korea University, Seoul, South Korea*

[2] *Department of Environmental Science, Hankuk University of Foreign Studies, Yongin, South Korea*

[3] *Air Quality Forecasting Center, Climate and Air Quality Research Department, National Institute of Environmental Research (NIER), Incheon, South Korea*

[4] *Department of Atmospheric Science, Pusan National University, Busan, South Korea*

* *Corresponding author*: Meehye Lee (meehye@korea.ac.kr)

Abstract

Nitrous acid (HONO), one of the reactive nitrogen oxides (NO_y), plays an important role in the formation of ozone (O_3) and fine aerosols ($PM_{2.5}$) in the urban atmosphere. In this study, a new simulation approach to calculate HONO mixing ratios using a deep neural technique based on measured variables was developed. The 'Reactive Nitrogen species simulation using Deep neural network (RND)' has been implemented in Python. The first version of RND (RNDv1.0) was trained, validated, and tested with HONO measurement data obtained in Seoul during the warm months from 2016 to 2019.

A k-fold cross validation and test results confirmed the performance of RND v1.0 with an Index Of Agreement (IOA) of 0.79 ~ 0.89 and a Mean Absolute Error (MAE) of 0.21 ~ 0.31 ppbv. The RNDv1.0 adequately represents the main characteristics of the measured HONO and thus, RND v1.0 is proposed as a supplementary model for calculating the HONO mixing ratio in a polluted urban environment.

1. Introduction

Surface ozone (O_3) pollution has been reported to be worsen over continental areas (Arnell et al., 2019;Monks et al., 2015;Varotsos et al., 2013;IPCC, 2014). In particular, a warmer climate is expected to increase surface O_3 concentrations and peak levels in polluted regions, depending on its precursor levels (IPCC 2021). As one of the short-lived climate pollutants (SLCPs), O_3 also interacts with the global temperature via positive feedback (Shindell et al., 2013;Myhre et al., 2017;Stevenson et al., 2013). Therefore, it is imperative to accurately predict the mixing ratios and variations of surface O_3. While operational models such as community multiscale air quality (CMAQ) have been used widely for this purpose, uncertainties still arise from poorly understood chemical mechanisms involving reactive nitrogen oxides (NOy) and volatile organic compounds (VOCs), and lack of their measurements (Mallet and Sportisse, 2006;Canty et al., 2015;Akimoto et al., 2019;Shareef et al., 2019;Cheng et al., 2022).

In the urban atmosphere, NO_y typically includes NO_x ($NO + NO_2$), HONO, HNO_3, organic nitrates (e.g., PAN), NO_3, N_2O_3, and particulate NO_3^-. These species are produced and recycled through photochemical reactions until they are removed through wet or dry deposition (Liebmann et al., 2018;Brown et al., 2017;Wang et al., 2020;Li et al., 2020). NO_y play an important role in critical environmental issues concerning the Earth's atmosphere, spanning from local air pollution to global climate change (Sun et al., 2011;Ge et al., 2019). The oxidation of NO to NO_2, and finally to HNO_3, is the backbone of the chemical mechanism producing ozone (O_3) and $PM_{2.5}$ (particulate matter of size $\leqslant$ 2.5 μm), and it determines the oxidization capacity of the atmosphere. Recently, as O_3 has increased along with a decrease in NO_x emission over many regions including East Asia, interest in the heterogeneous reaction of reactive nitrogen oxides, which is yet to be understood, has been newly raised (Brown et al., 2017;Stadtler et al., 2018). Currently, the lack of measurement of individual NO_y species hindered a comprehensive understanding of the heterogeneous reactions (Anderson et al., 2014;Wang et al., 2017b;Chen et al., 2018b;Akimoto and Tanimoto, 2021;Stadtler et al., 2018).

In particular, there are growing number of evidence for heterogeneous formation of HONO in relation to high $PM_{2.5}$ and O_3 occurrence in urban areas (e.g., (Li et al., 2021b). As

an OH reservoir, HONO will expedite the photochemical reactions involving VOCs and NOx in the early morning, leading to O_3 and fine aerosol formation. Nonetheless, its formation mechanism has not been elucidated clearly enough to be constrained in conventional photochemical models. In addition to the reaction of NO with OH (Bloss et al., 2021), various pathways of HONO formation have been suggested from laboratory experiments, field measurements, and model simulations: direct emissions from vehicles (e.g., (Li et al., 2021a) and soil (e.g.,(Bao et al., 2022), photolysis of particulate nitrate (e.g., (Gen et al., 2022), heterogeneous conversion of NO_2 on various aerosol surfaces (e.g., (Jia et al., 2020), ground surface (e.g.,(Meng et al., 2022), and microlayers of sea surface (e.g., (Gu et al., 2022). Among these, the heterogeneous reaction mechanism on the surface is of major interest in the recent HONO study.

HONO has been measured mostly during intensive campaigns in urban areas using various techniques such as a long path absorption photometer (LOPAP) (Kleffmann et al., 2006;Xue et al., 2019), chemical ionization mass spectrometry (CIMS) (Levy et al., 2014;Roberts et al., 2010), ion chromatography (IC) (VandenBoer et al., 2014;Gil et al., 2020;Ye et al., 2016;Xu et al., 2019), and quantum cascade tunable infrared laser differential absorption spectrometry (QC-TILDAS) (Lee et al., 2011;Gil et al., 2021). Of these methods, QC-TILDAS has served as a reference for intercomparison of measurement data from different techniques due to high time resolution and stability (Pinto et al., 2014). These studies reported the maximum HONO of several ppb levels at nighttime. In comparison, the model captured at most 67~90 % of the observed HONO in megacities such as Beijing (Tie et al., 2013;Liu et al., 2019).

In recent years, Machine Learning (ML) method has been adopted in the atmospheric science for pattern classification (e.g. New Particle Formation event) and forecasting and spatiotemporal modelling of O_3 and $PM_{2.5}$ (Arcomano et al., 2021;Shahriar et al., 2020;Krishnamurthy et al., 2021;Cui and Wang, 2021;Joutsensaari et al., 2018;Chen et al., 2018a;Kang et al., 2021). Among ML methods, the Neural Network (NN) architecture is widely used owing to its powerful ability to process large amounts of data, allowing improvement in the performance of conventional models through being integrated with physical equations (Reichstein et al., 2019;Schultz et al., 2021). As a NN architecture, a multi-layer artificial neural network, referred to as a Deep Neural Network (DNN), employs a statistical method that learn

non-linear relations in data and obtain the optimum solution for the target species without prior information on the physicochemical processes. DNN has advantages over other NN architecture such as Convolution NN (CNN) or Long-Short Term Memory (LSTM) because it works well for discrete spatiotemporal data. In general, the performance of DNN is similar to or better than other ML methods for small number of data as well as large data set (Baek and Jung, 2021;Dang et al., 2021;Sumathi and Pugalendhi, 2021).

When the DNN method is applied to atmospheric chemical constituents, it requires large amount of data for training and thus, the size of measurement data becomes a limiting factor for trace species such as HONO, which are not routinely measured such as O_3 or $PM_{2.5}$. In this regard, the daily average HONO mixing ratio was attempted to be estimated using ensemble ML models with satellite measurements (Cui and Wang, 2021). In comparison, the hourly HONO mixing ratio was calculated using a simple NN architecture with measured variables, which were thought to be deeply involved in the formation of HONO (Gil et al., 2021). The accuracy of the hourly HONO estimated from input variables such as aerosol surface areas and mixed layer height was better than the daily HONO estimate.

The aim of this study is to develop a user-friendly 'Reactive Nitrogen species simulation using DNN' model (RNDv1.0) that estimates HONO mixing ratios from real-time measurements of criteria pollutants and meteorological parameters and is ultimately to be incorporated into operational models that forecast urban air quality. Since this study is the first attempt to calculate the HONO mixing ratio using RNDv1.0, the entire construction process is described in detail, and the performance is evaluated by comparing the results with simulations using a commonly used model and observations over several years.

2. Model description

The development of RNDv1.0 model follows the systematic steps similar to a general machine learning model construction workflow, including collecting data, preprocessing data, building the DNN, training and validating the model, and testing the performance of the model (Figure 1). The RNDv1.0 was written in Python and necessary libraries to build and operate

121 RNDv1.0 are listed in Table 1. The dataset used to train-test-validation can be downloaded from
122 Gil et al., 2021.

123

124 **2.1. Collection of measurement data for model construction**

125

126   As the first step constructing the RNDv1.0, measurement data were obtained including
127 HONO, reactive gases, and meteorological parameters. It is noteworthy that the HONO
128 measurement data is for model construction and is not required to run the RND model. The
129 HONO mixing ratio was measured using a Quantum Cascade – Tunable Infrared Laser
130 Differential Absorption Spectrometer (QC-TILDAS) system in Seoul during May–June 2016,
131 June 2018, and April-June 2019 (Lee et al., 2011;Gil et al., 2021). When testing and evaluating
132 atmospheric HONO measurement methods, QC-TILDAS has been chosen as the reference
133 method for comparing ambient HONO mixing ratios measured using several different
134 techniques owing to its advantages of low detection limits (~ 0.1 ppbv) and high temporal
135 resolution (Pinto et al., 2014). More details on measurements can be found elsewhere (Gil et
136 al., 2021).

137   HONO was measured at Olympic Park (37.52°N, 127.12°E) during the Korea-United
138 States Air Quality (KORUS-AQ) study in 2016 (Kim et al., 2020;Gil et al., 2021), at the campus
139 of Korea University (37.59°N, 127.03°E) in 2018, and at the site near the campus (37.59°N,
140 127.08°E) in 2019 (NIER, 2020) (Figure S1). Although measurements were made at three sites,
141 O_3 and $PM_{2.5}$ levels have been known to be greatly influenced by the synoptic circulation
142 throughout the Korean peninsula (Peterson et al., 2019;Jordan et al., 2020), and the Korea
143 University campus and Olympic Park have served as measurement sites representing the air
144 quality of Seoul. In addition to HONO, trace gases including O_3, NO_2, CO, and SO_2 and
145 meteorological parameters including temperature (T), relative humidity (RH), wind speed (WS)
146 and direction (WD) were measured. Note that HONO was not significantly correlated with any
147 of these variables (Figure S2). The measurement statistics are presented in Table 2 and Table
148 S1. Briefly summarizing, the 10th and 90th percentile mixing ratios of HONO, NO_2, and O_3 are
149 0.3 ppbv and 1.9 ppbv, 10.7 ppbv and 48.2 ppbv, and 12.0 ppbv and 80.9 ppbv, respectively for
150 the entire experiment periods.

151

2.2. Data preprocessing

153

In the next step, the observation data set was prepared for RNDv1.0 model construction. As input variables, hourly measurements of chemical and meteorological parameters are used, including the mixing ratios of O_3, NO_2, CO, and SO_2, along with temperature (T), relative humidity (RH), wind speed (WS), wind direction (WD), and solar zenith angle (SZA) to estimate the target species, HONO, as the output. Wind direction in degrees were converted to a cosine value for continuity. As a last step in data processing, missing values were filtered out from the input dataset. Finally, 50.7 % of all available measurement data (1636) were used to construct the RNDv1.0 in this study.

Since the measurements of these nine variables vary over a wide range in different units, they were normalized to avoid bias during the calculations. Among the widely used normalization methods, '*min-max scaling*' method was adopted and input variables were normalized against the minimum and maximum values in this study (Eq. 1):

166

$$x_{sca} = \frac{x_{raw} - F_2(X)}{F_1(X)}, \tag{1}$$

168

where x_{raw} is raw data, x_{sca} is scaled value, and F_1 and F_2 are scale factors of input variable (X), which are listed in Table 2.

171

2.3. Neural network architecture and hyperparameters

173

At this stage, the network is built to calculate HONO using those input variables. The RNDv1.0 is composed of five hidden layers (Figure 2), which employed an exponential linear unit (ELU) as an activation function (Eq. 2).

177

178        $\text{ELU}: \phi(x) = \begin{cases} e^x - 1 \ (x < 0) \\ \quad x \ (x \geq 0) \end{cases}.$ (2)

179

180   In a DNN, an activation function creates a nonlinear relationship between an input

181 variable and an output variable. When constructing a DNN model, an ELU has the advantage

182 of a fast-training process and better performance in handling negative values than other

183 activation functions (Wang et al., 2017a;Ding et al., 2018). In addition, the mean squared error

184 and Adam optimizer were applied as loss function and optimize function, respectively. The

185 learning rate, epoch, and batch were set to 0.01, 100, and 32, respectively.

186

187 **2.4. Model training**

188

189   The RNDv1.0 model was trained, validated, and tested with HONO measurements obtained

190 during May ~ June in 2016 and 2019, in June 2018, and in April 2019, respectively (Figure 3).

191 The number of data used for train, validation, and test were 1122, 381, and 133, respectively.

192   With the hyperparameters specified in previous section, the performance of the model was

193 firstly validated using the k-fold cross-validation method, which is especially useful when the

194 size of dataset is small (Bengio and Grandvalet, 2003). In the k-fold cross-validation method

195 (Figure 3), the entire data is randomly divided into k subsets, of which k-1 sets were used for

196 training and the rest one was used for validation. k was set to 5 in this study. The accuracy was

197 determined by Index Of Agreement (IOA) and Mean Absolute Error (MAE) expressed by the

198 following equation (Eq. 3, Eq. 4):

199

200        $\text{IOA} = 1 - \dfrac{\sum_{i=1}^{n}(O_i - P_i)^2}{\sum_{i=1}^{n}(|P_i - \bar{O}| + |O_i - \bar{O}|)^2},$ (3)

201        $\text{MAE} = \dfrac{\sum_{i=1}^{n}|O_i - P_i|}{n},$ (4)

202

203   where O_i, P_i, $\bar{O}$, and n are the observed value, predicted value, average of the observed

204 values, and number of nodes, respectively. The overall accuracy of

As IOA and MAE vary according to the number of nodes, they were calculated for the measured ($HONO_{obs}$) and calculated ($HONO_{mod}$) mixing ratios by varying the number of nodes from 0 to 100 in each hidden layer. The best performance was found with 41 nodes, with which the averaged IOA and MAE were 0.89 ± 0.01 (mean $\pm$ standard deviation) and 0.31 ± 0.02 ppbv, respectively (Figure 4). The high level of IOA and low MAE demonstrates that the performance of RNDv1.0 model is adequate, and it is capable of simulating the ambient HONO mixing ratio using the routinely measured criteria pollutants and meteorological parameters. In particular, MAE was commensurate with the detection limit of HONO measurement.

After the network validation, HONO mixing ratio was calculated for May ~ June in 2016 and 2019, and the model results were compared with the measured values (Figure 5). The average mixing ratios of measured and calculated HONO was 0.94 ppbv and 0.89 ppbv in 2016, and 1.02 ppbv and 0.96 ppbv in 2019, respectively. The MAE and IOA of the measurement and calculation were 0.27 ppbv and 0.90 in 2016, and 0.29 ppbv and 0.91 in 2019, respectively, demonstrating the ability of the RNDv1.0 to simulate ambient HONO levels. In both cases, however, the model slightly underestimated the highest and lowest HONO mixing ratios, which is mainly due to the limited number of data used for training, but also related to the intrinsic nature of DNN. The model calculation well captured the diurnal variation of ambient HONO with a slight underestimation (Figure 6). In addition, the correlation between $HONO_{mod}$ and $HONO_{obs}$ was better in 2019 (MAE = 0.06 ppbv) than in 2016 (MAE = 0.08 ppbv). Since the MAE of the two cases was far below the detection limit of HONO measurements (~ 0.1 ppbv), the RNDv1.0 is considered suitable for simulating HONO in urban areas.

Next, the HONO calculated in RNDv.1.0 was compared with observations and results from CMAQ (Community Multi-scale Air Quality Model, v5.3.1) simulations during the KORUS-AQ study (May~June 2016) (Figure 7). More information on CMAQ modeling can be found elsewhere (Appel et al., 2021). While the results of RNDv.1.0 reasonably traced the observed variations (IOA = 0.90), the CMAQ severely underestimated the measured HONO concentration (IOA = 0.44). These results demonstrate the performance and efficacy of RNDv1.0 in calculating the ambient HONO mixing ratio that are poorly reproduced in conventional operating models.

2.5. Influence of input variables on HONO concentration

236

A simple bootstrapping test was conducted to evaluate the relative importance of the input variable to HONO concentration. In this analysis, each variable was set to zero and MAE was calculated as an evaluation metrics (Kleinert et al., 2021). Of nine input variables, NO_2 was found to have the most significant influence on HONO concentration, followed by RH, temperature, and solar zenith angle (Table 4). The highest MAE of 0.59 ppbv can be considered as the maximum uncertainty of RNDv1.0 due to the input variable.

The result of bootstrap test is in good agreement with those of our previous study (Gil et al., 2021), where more variables such as aerosol surface area and mixing layer height were incorporated into the model, highlighting the crucial role of precursor gases and heterogeneous conversion in HONO formation. Therefore, these results demonstrate that the RND model constructed from routinely measured criteria pollutants and meteorological parameters sufficiently captured the HONO variability in the urban atmosphere.

2.6. Model validation and test

Finally, the RND model was validated and tested against the measurement data obtained in June 2018 and April 2019. The calculated HONO mixing ratios are compared with those measured in Figure 8, and their MAE and IOA are listed in Table 3. The two sets of model performance test showed that the model reasonably traced what was observed. As the validation result of RND, the MAE and IOA of the calculated and measured in June 2018 are comparable to those of 2016~2019 result. However, the MAE and IOA of the April 2019 measurements were relatively poor compared to the validation results. Especially, the MAE of the April 2019 is about twice as high as those of validation.

In these two test periods, HONO levels were lower than those observed on validation days (Figure 8), and the model tended to overestimate high HONO concentrations. It is possibly due to the variability of HONO that is not fully captured by RNDv1.0 using 9 input variables. As stated above, heterogeneous reactions intimately involved in HONO formation are not considered in RNDv1.0. More importantly, the annual variability of criteria pollutants such as

265 PM$_{2.5}$ has increased in recent years. Particularly in 2019, the monthly average PM$_{2.5}$ mass
266 concentration was lower in April (21 μg m^{-3}) than in May (29 μg m^{-3}), unlike normal years.
267 Given that the test result is within the uncertainty range of the model that is primarily
268 determined by NO$_2$ (Table 4), RNDv1.0 will be applicable to urban environments under various
269 conditions.

270

271 **3. Operation and application of RNDv1.0**

272

273 The RNDv1.0 package is provided as an operational model, .h5 files that can be opened in
274 Python. To run the RNDv1.0, the measurement data for nine input variables are required and
275 need to be properly prepared as described in Section 2.2. A sample of preprocessed input dataset
276 is provided as a .csv file (Dataset_for_model.csv). Once the input data is ready, open the
277 RNDv1.0 with input data files using the code provided in the example (Figure S3). Then, RND
278 v1.0 calculates and presents the HONO results as scaled values (x_{sca}), which will be finally
279 converted to HONO mixing ratio (ppbv) by the two scale factors in Table 2 (Eq. 5):

280

281 $$HONO \text{ (ppbv)} = HONO_{sca} \times F_1(HONO) + F_2(HONO). \qquad (5)$$

282

283 The HONO calculated by Eq. 5 can be applied to an urban photochemical cycle simulation.
284 It is already known that the photolysis of HONO is a major source of OH radicals in the early
285 morning when the OH level is low, and this OH affects daytime O$_3$ formation through
286 photochemical reactions with VOCs and NO$_x$, which are primarily emitted during morning rush
287 hour in urban areas. In addition, the OH produced from HONO promotes the photochemical
288 oxidation of SO$_2$ and VOCs, leading to aerosol formation. However, the HONO formation
289 mechanism is still poorly understood, hindering O$_3$ and fine aerosols as well as HONO from
290 being correctly simulated in conventional photochemical models.

291 The 0-Dimension Atmospheric Modelling (F0AM) utilizing the MCM v3.3.1 chemical
292 reaction mechanisms (Wolfe et al., 2016), can be used to simulate the diurnal variation of O$_3$
293 with the measurements of several reactive gases (NO, NO$_2$, CO, HCHO, VOCs, and HONO).

294 Detailed information about F0AM can be found in
295 (https://sites.google.com/site/wolfegm/models) and in previous works published elsewhere
296 (Wolfe et al., 2016; Gil et al., 2020). When the F0AM model is run without HONO, it is not
297 able to reproduce the concentration and diel cycle of the observed O_3 (Figure 9). In comparison,
298 the model simulates the O_3 well within 2 ppbv when adding HONO, which is the product of
299 RND v1.0. This is mainly due to the missing OH produced by HONO photolysis in the early
300 morning. Its production rate is estimated to be 0.57 pptv s^{-1}, contributing approximately 2.28
301 pptv to OH budget during 06:00 ~ 11:00 (LST) (Gil et al., 2021). Given that OH is mainly
302 produced from the photolysis of O_3 under high sun, the early morning source of OH will
303 expedite the photochemical cycle involving NO_x and VOCs, promoting O_3 and secondary
304 aerosol formation. Since the presence of HONO in the photochemical model allows for accurate
305 estimation of OH radicals, the incorporation of RNDv1.0 into conventional models will
306 improve their overall performance.

307

308   **4. Summary and implications**

309

310   In this study, we developed the RND model to calculate the mixing ratio of NO_y in an urban
311 atmosphere using a DNN along with measurement data. The target species of RNDv1.0 is
312 HONO, and its mixing ratio is calculated using criteria pollutants including O_3, NO_2, CO, and
313 SO_2, and meteorological variables including T, RH, WS, and WD, along with the SZA. These
314 variables are routinely measured through monitoring networks. The RNDv1.0 was trained and
315 validated using the HONO measurements obtained in Seoul by adopting a k-fold cross
316 validation method and tested with other HONO datasets measured using the same instrument.
317 The validation and test results demonstrate that RNDv1.0 adequately captures the characteristic
318 variation of HONO and confirms the efficacy of RND v1.0.

319   RNDv1.0 was constructed using the measurement made in a high NO_x environment during
320 early summer (May–June). It is noteworthy that in this period, the HONO mixing ratio was
321 raised above 3 ppbv with the highest O_3 levels under stagnant conditions. If RNDv1.0 is applied
322 to areas under significant influence of outflows, the model possibly overestimates or
323 underestimate the level of HONO without detailed information such as nanoparticles. In the

previous study, the formation of HONO was shown to be intimately related with surface areas of submicron particles (Gil et al., 2021). Nevertheless, the HONO concentration produced from RNDv1.0 with routine measurements provides the benefit of relatively inexpensive test for measurement quality control, location selection, and supports the data used for traditional chemistry model based on the current knowledge of the urban photochemical cycle. Therefore, it is reasonable to argue that RNDv1.0 can serve as a supplementary tool for conventional forecasting models. As attempts are currently being made to estimate ground HONO from satellite observations (Clarisse et al., 2011;Theys et al., 2020;Armante et al., 2021), RNDv1.0 will also be useful for validating satellite-derived HONO by supplementing measurement data.

5. Acknowledgements

This study was supported by the National Research Foundation of Republic of Korea (2020R1A2C3014592) and Korea Institute of Science and Technology (KIST2E31650-22-P019).

6. Code availability

The RND model codes (.h5 files) with preprocessed sample data can be downloaded from (Gil, 2021).

7. Author contributions

JG and ML designed the manuscript and developed the model code. JK, GL, and JA provided HONO measurements and CK provided CMAQ model data. All the authors contributed to the manuscript.

351 **8. Competing interests**

352

353 The authors declare that they have no conflict of interest.

354

355

  Figures and Tables
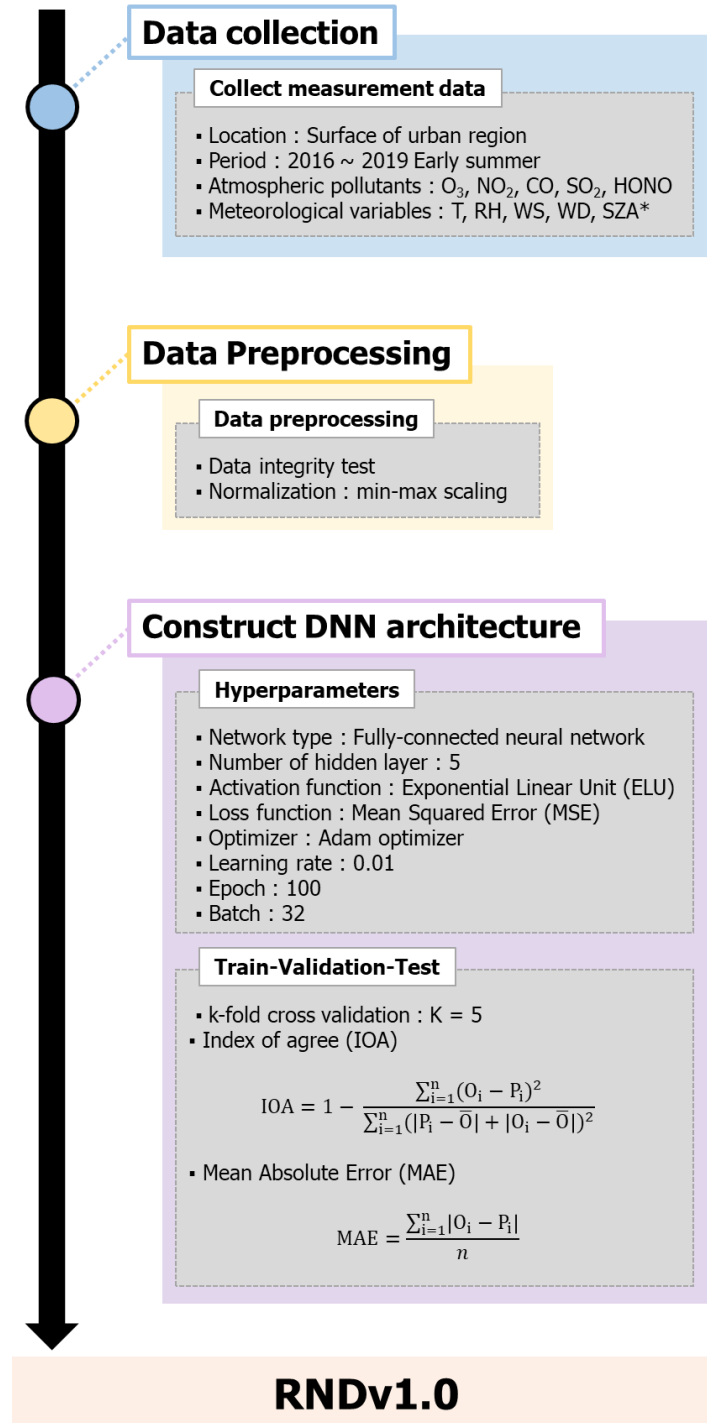
  Figure 1. The main processes for configuring the RNDv1.0 (*: calculated values)
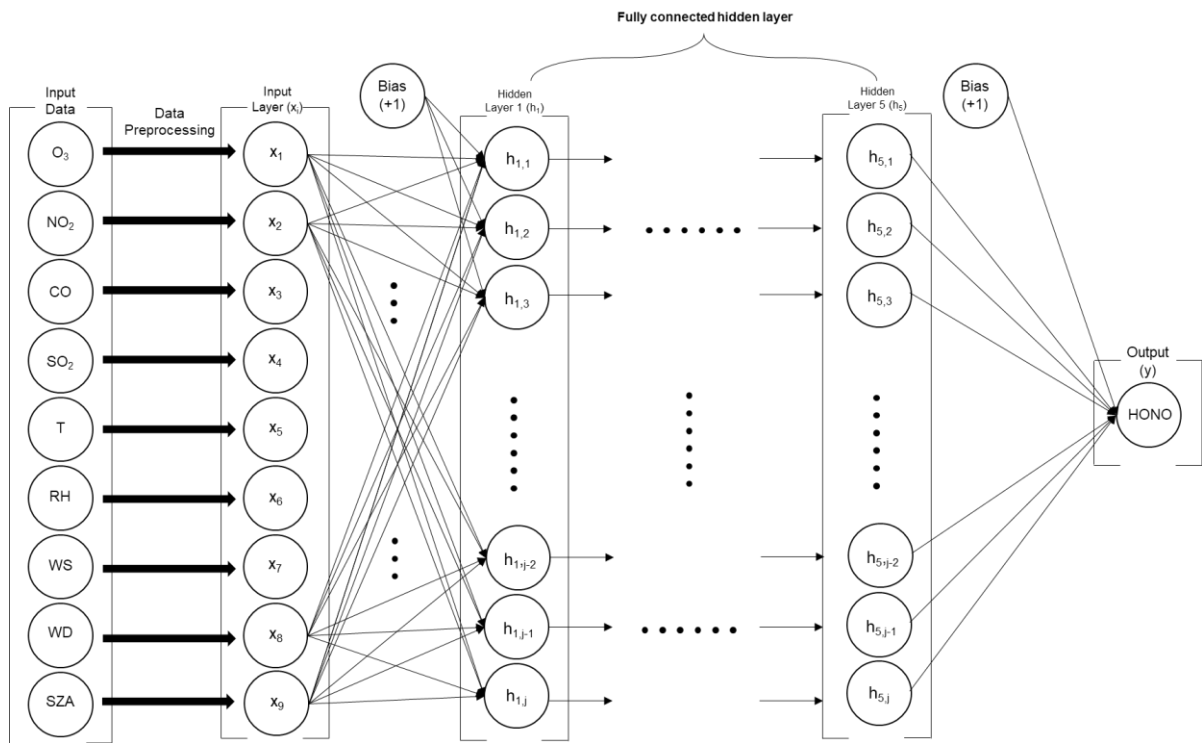
360

361   **Figure 2.** The structure of deep neural network built for RND v1.0.

362

363

364
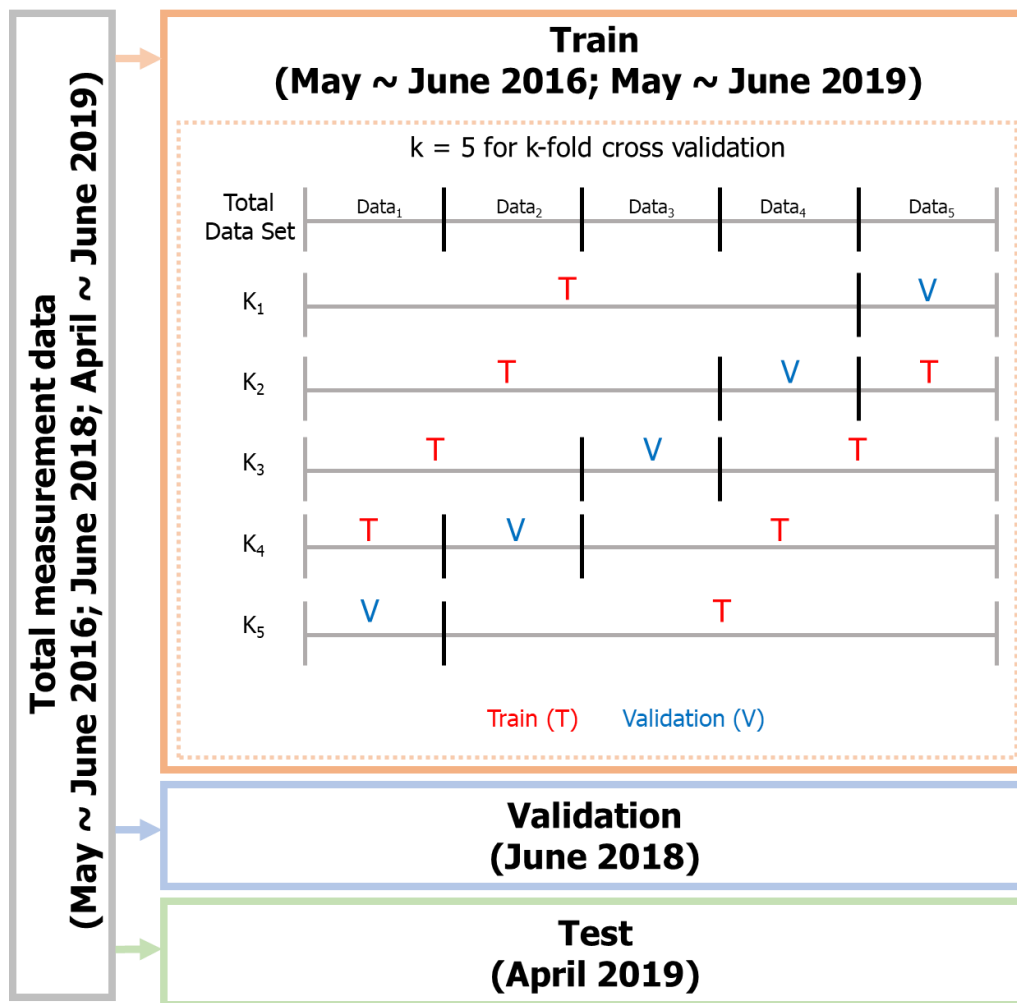
Figure 3. Design of training, validation, and test to build RNDv1.0 using measurement data. The k-fold cross validation were performed using randomly divided five subsets of training data set.

365

366

367

368
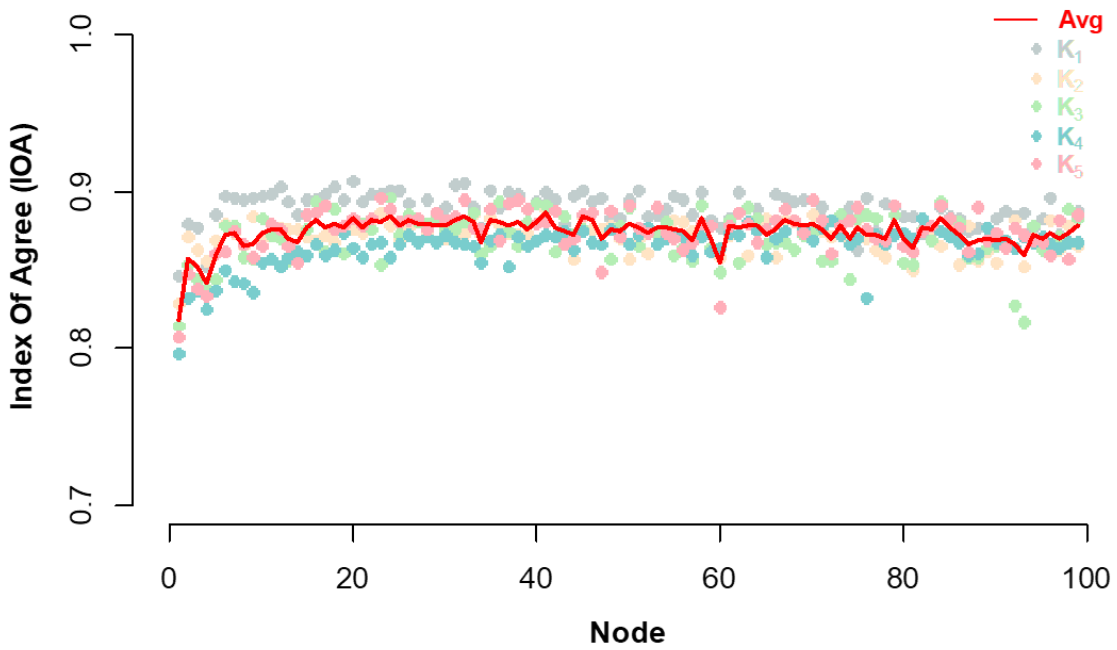
369

370 **Figure 4.** Index Of Agreement (IOA) for k-fold cross validation. Solid circle and red line

371 represent IOA for each validation (k=5) and the average of 5 validation sets at each node number.

372
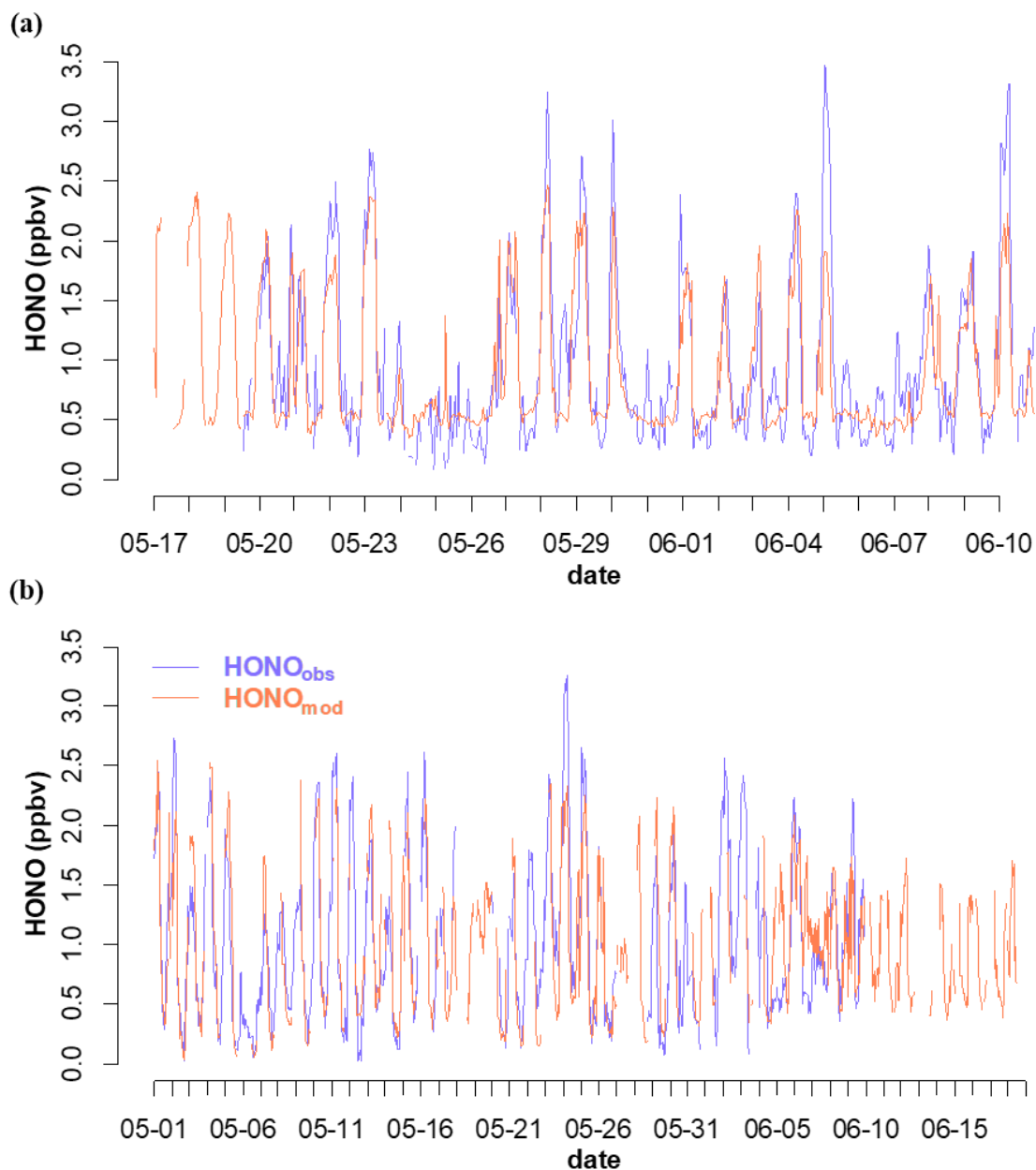
373

374 **Figure 5.** Comparison between the measured (HONO_obs) and calculated (HONO_mod) HONO

375 mixing ratios in Seoul during May~June in (a) 2016 and (b) 2019. The blue and red lines

376 indicate the measured and calculated HONO mixing ratio, respectively.

377
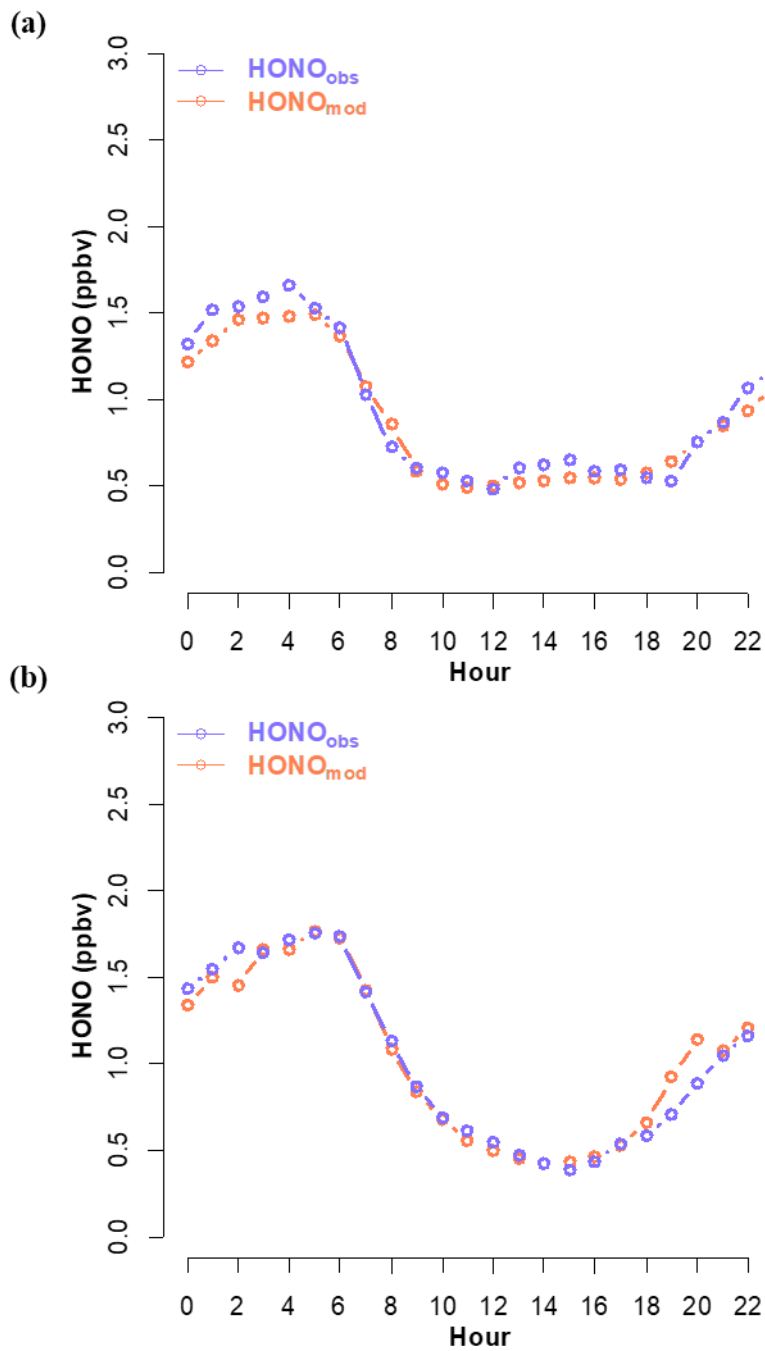
379 **Figure 6**. Average diurnal variations of the measured (HONO$_{obs}$) and the calculated (HONO$_{mod}$)

380 HONO mixing ratios in Seoul during May ~ June in (a) 2016 and (b) 2019.

381

382

383
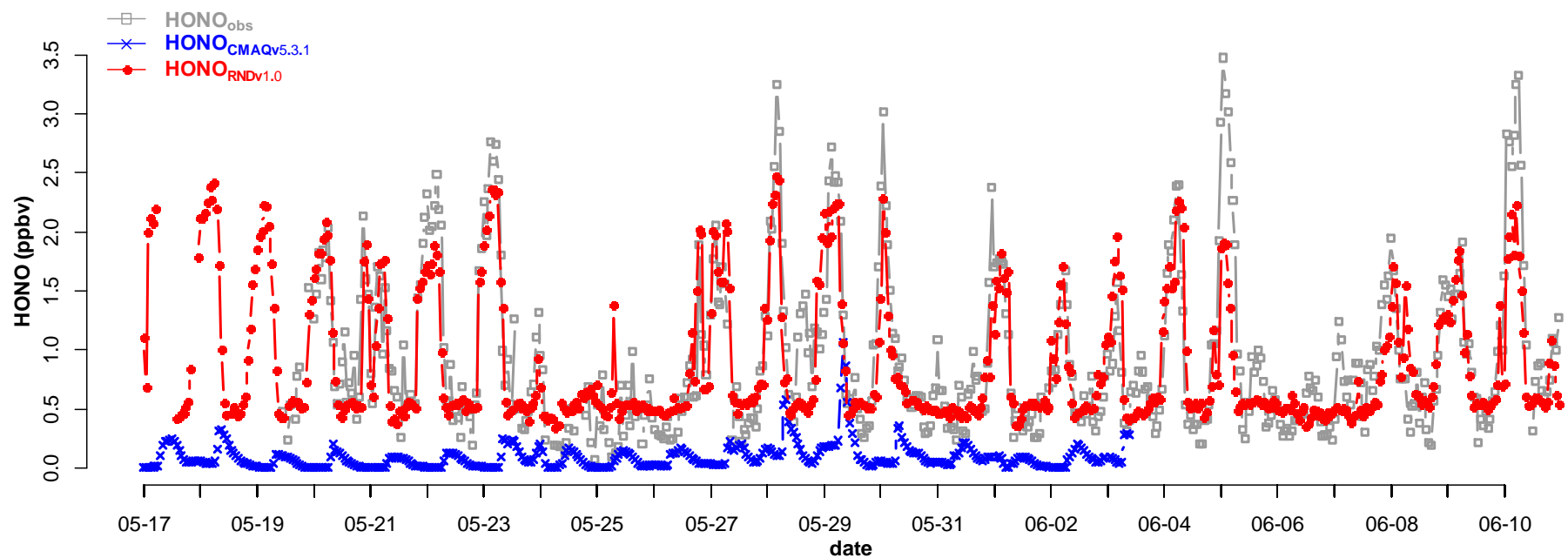
Figure 7. During the KORUS-AQ campaign (May-June 2016), HONO mixing ratios calculated using RNDv1.0 (red dot) are compared with those

385 observed (gray square) and calculated using CMAQv5.3.1 (blue cross).
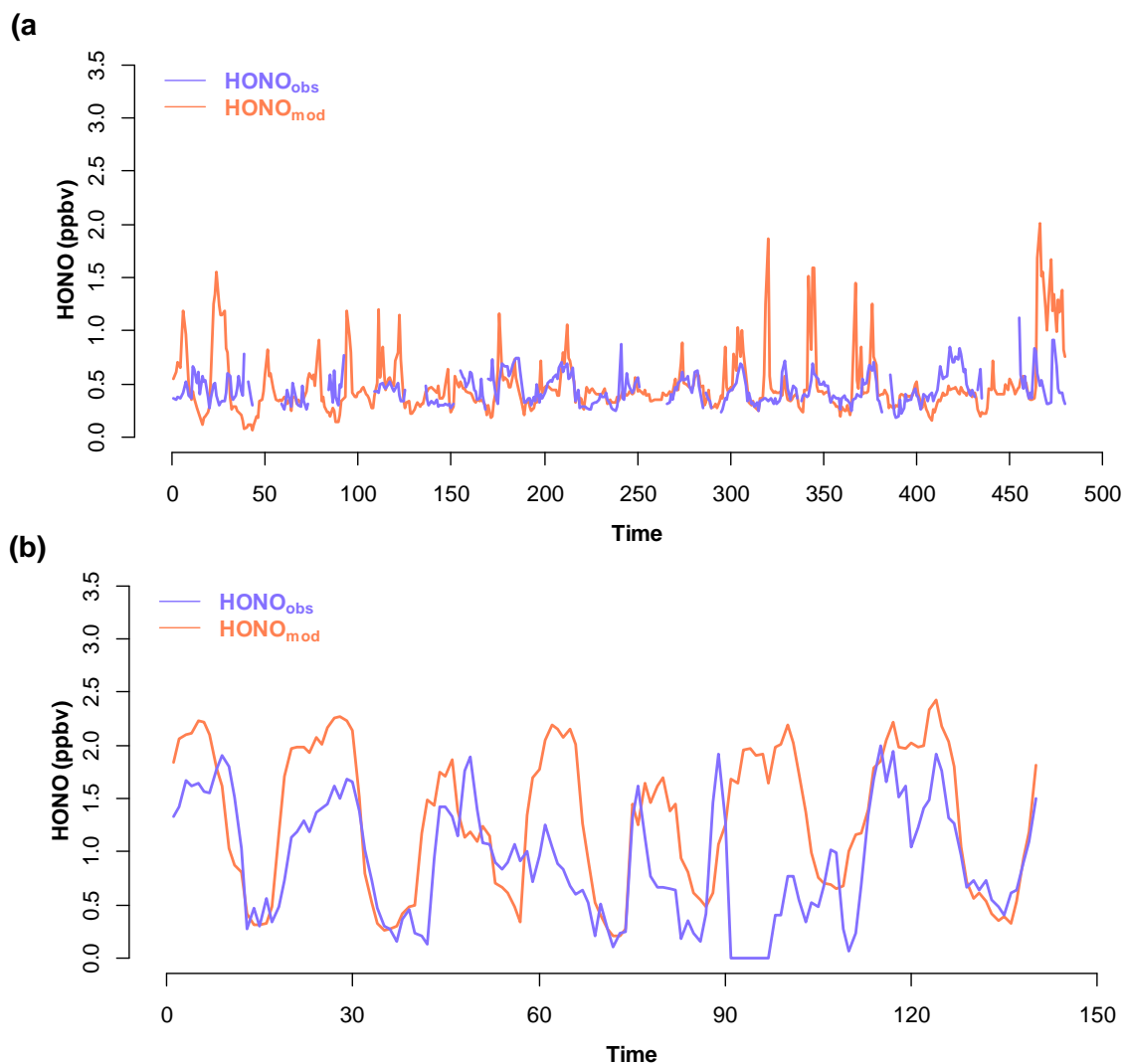
386

387 **Figure 8.** Comparison between the measured (HONO_obs) and calculated (HONO_mod) HONO

388 mixing ratios in Seoul during (a) June 2018 and (b) April 2019. The blue and red lines indicate

389 the measured and calculated HONO mixing ratio, respectively. The x axis indicates the hour

390 from the beginning of the experiment, which is (a) 00:00 on 1st June 2018 and (b) 00:00 on 12th

391 April 2019.

392

393
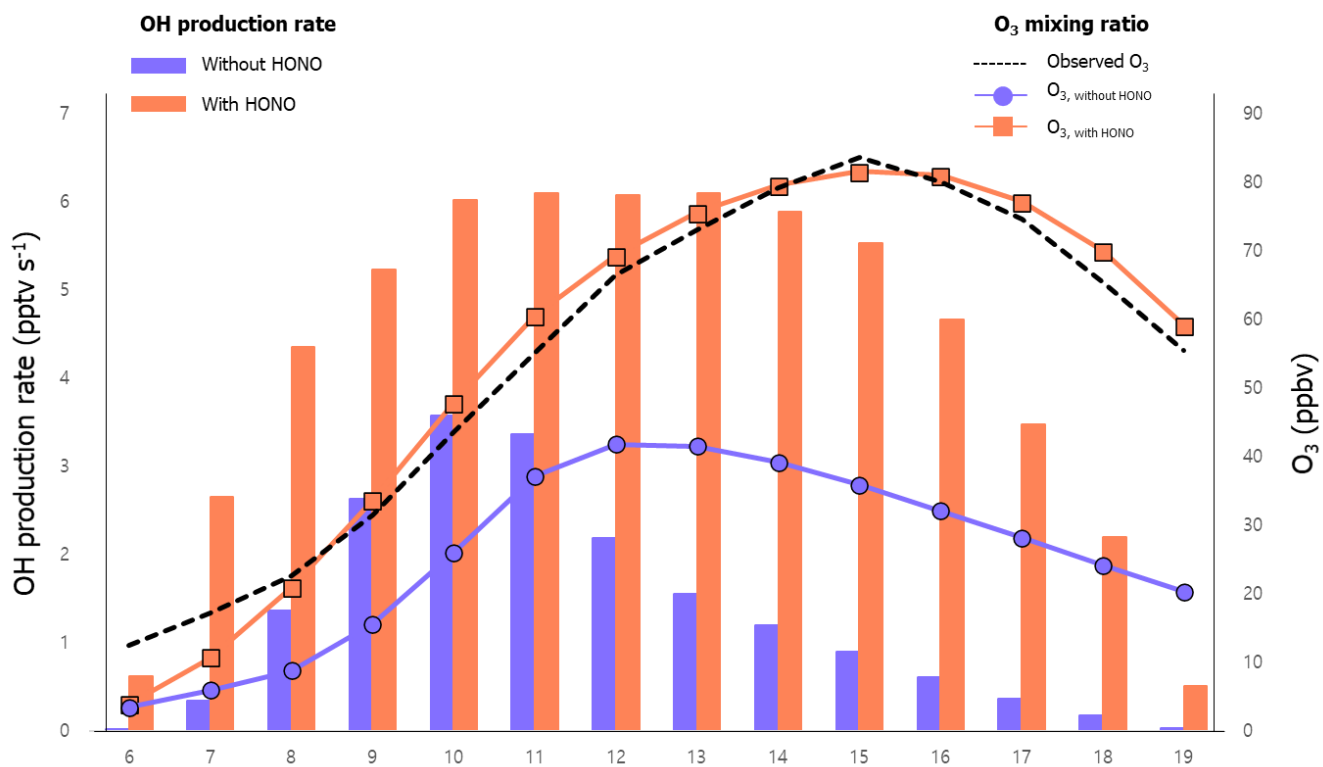
Figure 9. For June 2016, diurnal variations of O_3 (line) and OH production rate (bar) calculated

from the F0AM photochemical model with (orange) and without (blue) HONO estimated from

the RNDv1.0 model. The measured O_3 is compared with the calculated.

397

398 **Table 1.** Resources for constructing RND model.

	Version	Remark
Python	v3.8.3	
CUDA	v10.1	*If using GPU
CuDNN	v7.6.5	*If using GPU
Tensorflow	v2.3.0	*Python library*
Keras	v2.4.3	*Python library*
Pandas	v1.0.5	*Python library*
Numpy	v1.18.5	*Python library*

399 *GPU denotes graphic processing unit

400 **Table 2**. Input variables and their concentrations ($10^{th} \sim 90^{th}$ percentile), coverage, and scale
401 factors for RNDv1.0 model. Measurements were made in Seoul during May ~ June in 2016 and
402 2019.

	$10^{th}\sim90^{th}$ percentile (unit)	Coverage (%)	Scale Factor1 (F_1)*	Scale Factor 2 (F_2)**
Input Variables				
O_3	12.1 ~ 90.4 (ppbv)	95.5	204.738	0.842
NO_2	11.0 ~ 48.6 (ppbv)	80.6	79.925	2.375
CO	252 ~ 743 (ppbv)	95.1	975.248	137.253
SO_2	1.9 ~ 6.4 (ppbv)	95.6	12.479	0.958
Solar Zenith Angle	22.7 ~ 118.4 (º)	100.0	112.317	14.195
Temperature	15.9 ~ 26.7 (°C)	99.4	24.240	8.610
Relative Humidity	29.2 ~ 79.1 (%)	99.4	88.545	10.555
Wind Speed	0.2 ~ 3.7 (m/s)	99.4	7.581	0.005
Wind Direction	45.4 ~ 287.5 (º)	99.4	359.565	0.235
Output Variables				
HONO	0.3 ~ 2.0 (ppbv)	81.1%	3.447	0.013

403 * Maximum – Minimum

404 ** Minimum value

405

406 **Table 3.** The result of validation and test of RNDv1.0 model using measurement data.

Measurement data	Validation		Test	
	MAE (ppbv)	IOA	MAE (ppbv)	IOA
May 2016*	0.26	0.93		
June 2016*	0.29	0.86		
June 2018	0.21	0.79		
April 2019			0.56	0.65
May 2019*	0.26	0.93		
June 2019*	0.36	0.76		

407 *Re-using the data already used for training

408

409 **Table 4.** The result of bootstrap test of measurement data used to train RNDv1.0 model. The
410 greater the MAE, the greater the influence of variable.

Variable (X)	MAE (ppbv)
-	0.28
O_3	0.29
NO_2	0.59
CO	0.37
SO_2	0.34
Solar zenith Angle (SZA)	0.41
Temperature (T)	0.52
Relative humidity (RH)	0.52
Wind speed (WS)	0.34
Wind direction (WD)	0.29

411

412

Reference

Akimoto, H., Nagashima, T., Li, J., Fu, J. S., Ji, D., Tan, J., and Wang, Z.: Comparison of surface ozone simulation among selected regional models in MICS-Asia III–effects of chemistry and vertical transport for the causes of difference, Atmospheric Chemistry and Physics, 19, 603-615, 2019.

Akimoto, H., and Tanimoto, H.: Review of Comprehensive Measurements of Speciated NOy and its Chemistry: Need for Quantifying the Role of Heterogeneous Processes of HNO3 and HONO, Aerosol and Air Quality Research, 21, 200395, 2021.

Anderson, D. C., Loughner, C. P., Diskin, G., Weinheimer, A., Canty, T. P., Salawitch, R. J., Worden, H. M., Fried, A., Mikoviny, T., and Wisthaler, A.: Measured and modeled CO and NOy in DISCOVER-AQ: An evaluation of emissions and chemistry over the eastern US, Atmospheric Environment, 96, 78-87, 2014.

Appel, K. W., Bash, J. O., Fahey, K. M., Foley, K. M., Gilliam, R. C., Hogrefe, C., Hutzell, W. T., Kang, D., Mathur, R., and Murphy, B. N.: The Community Multiscale Air Quality (CMAQ) model versions 5.3 and 5.3. 1: system updates and evaluation, Geoscientific Model Development, 14, 2867-2897, 2021.

Arcomano, T., Szunyogh, I., Wikner, A., Pathak, J., Hunt, B. R., and Ott, E.: A Hybrid Approach to Atmospheric Modeling that Combines Machine Learning with a Physics-Based Numerical Model, Journal of Advances in Modeling Earth Systems, e2021MS002712, 2021.

Armante, R., Perrin, A., Kwabia Tchana, F., and Manceron, L.: The ν4 bands at 11 μm: linelists for the Trans-and Cis-conformer forms of nitrous acid (HONO) in the 2019 version of the GEISA database, Molecular Physics, e1951860, 2021.

Arnell, N. W., Lowe, J. A., Challinor, A. J., and Osborn, T. J.: Global and regional impacts of climate change at different levels of global temperature increase, Climatic Change, 155, 377-391, 2019.

Baek, W.-K., and Jung, H.-S.: Performance Comparison of Oil Spill and Ship Classification from X-Band Dual-and Single-Polarized SAR Image Using Support Vector Machine, Random Forest, and Deep Neural Network, Remote Sensing, 13, 3203, 2021.

Bao, F., Cheng, Y., Kuhn, U., Li, G., Wang, W., Kratz, A. M., Weber, J., Weber, B., Pöschl, U., and Su, H.: Key Role of Equilibrium HONO Concentration over Soil in Quantifying Soil–Atmosphere HONO Fluxes, Environmental science & technology, 2022.

Bengio, Y., and Grandvalet, Y.: No unbiased estimator of the variance of K-fold cross-validation, Citeseer, 2003.

Bloss, W. J., Kramer, L., Crilley, L. R., Vu, T., Harrison, R. M., Shi, Z., Lee, J. D., Squires, F. A., Whalley, L. K., and Slater, E.: Insights into air pollution chemistry and sulphate formation from nitrous acid (HONO) measurements during haze events in Beijing, Faraday Discussions, 226, 223-238, 2021.

Brown, S. S., An, H., Lee, M., Park, J.-H., Lee, S.-D., Fibiger, D. L., McDuffie, E. E., Dubé, W. P., Wagner, N. L., and Min, K.-E.: Cavity enhanced spectroscopy for measurement of nitrogen oxides in the Anthropocene: results from the Seoul tower during MAPS 2015, Faraday discussions, 200, 529-557, 2017.

Canty, T., Hembeck, L., Vinciguerra, T., Anderson, D., Goldberg, D., Carpenter, S., Allen, D., Loughner, C., Salawitch, R., and Dickerson, R.: Ozone and NO x chemistry in the eastern US: evaluation of CMAQ/CB05 with satellite (OMI) data, Atmospheric Chemistry and Physics, 15, 10965-10982, 2015.

Chen, G., Li, S., Knibbs, L. D., Hamm, N. A., Cao, W., Li, T., Guo, J., Ren, H., Abramson, M. J., and Guo, Y.: A machine learning method to estimate PM2. 5 concentrations across China with remote sensing, meteorological and land use information, Science of the Total Environment, 636, 52-60, 2018a.

Chen, Y., Wolke, R., Ran, L., Birmili, W., Spindler, G., Schröder, W., Su, H., Cheng, Y., Tegen, I., and Wiedensohler, A.: A parameterization of the heterogeneous hydrolysis of N_2O_5 for mass-based aerosol models: improvement of particulate nitrate prediction, Atmos. Chem. Phys, 18, 673-689, 2018b.

Cheng, P., Pour-Biazar, A., White, A. T., and McNider, R. T.: Improvement of summertime surface ozone prediction by assimilating Geostationary Operational Environmental Satellite cloud observations, Atmospheric Environment, 268, 118751, 2022.

Clarisse, L., R'Honi, Y., Coheur, P. F., Hurtmans, D., and Clerbaux, C.: Thermal infrared nadir observations of 24 atmospheric gases, Geophysical Research Letters, 38, 2011.

Cui, L., and Wang, S.: Mapping the daily nitrous acid (HONO) concentrations across China during 2006-2017 through ensemble machine-learning algorithm, Science of The Total Environment, 147325, 2021.

Dang, C., Liu, Y., Yue, H., Qian, J., and Zhu, R.: Autumn crop yield prediction using data-driven approaches:-support vector machines, random forest, and deep neural network methods, Canadian Journal of Remote Sensing, 47, 162-181, 2021.

Ding, B., Qian, H., and Zhou, J.: Activation functions and their characteristics in deep neural networks, 2018 Chinese control and decision conference (CCDC), 2018, 1836-1841.

Ge, B., Xu, X., Ma, Z., Pan, X., Wang, Z., Lin, W., Ouyang, B., Xu, D., Lee, J., and Zheng, M.: Role of Ammonia on the Feedback Between AWC and Inorganic Aerosol Formation During Heavy Pollution in the North China Plain, Earth and Space Science, 6, 1675-1693, 2019.

Gen, M., Liang, Z., Zhang, R., Mabato, B. R. G., and Chan, C. K.: Particulate nitrate photolysis in the atmosphere, Environmental Science: Atmospheres, 2022.

Gil, J., Son, J., Kang, S., Park, J., Lee, M., Jeon, E., and Shim, M.: HONO measurement in Seoul during Summer 2018 and its Impact on Photochemistry, Journal of Korean Society for Atmospheric Environment, 36, 579-588, 10.5572/KOSAE.2020.36.5.579, 2020.

Gil, J.: RNDv1.0 and example, https://doi.org/10.5281/zenodo.5540180, in, Zenodo, 2021.

Gil, J., Kim, J., Lee, M., Lee, G., Ahn, J., Lee, D. S., Jung, J., Cho, S., Whitehill, A., Szykman, J., and Lee, J.: Characteristics of HONO and its impact on O3 formation in the Seoul Metropolitan Area during the Korea-US Air Quality study, Atmospheric Environment, 2021, https://doi.org/10.1016/j.atmosenv.2020.118182., 2021.

Gu, R., Wang, W., Peng, X., Xia, M., Zhao, M., Zhang, Y., Liu, Y., Shen, H., Xue, L., and Wang, T.: Nitrous acid in the polluted coastal atmosphere of the South China Sea: Ship emissions, budgets, and impacts, Science of The Total Environment, 153692, 2022.

IPCC: Summary for policymakers. In:Climate Change 2014: Impacts, Adaption, and Vulnerability. Part A: Global and Sectoral Aspects. Contribution of Working Group II to the Fifth Assessment Report of the Intergovernmental Panel on Climate Change [Field, C.B., V.R. Barros, D.J. Dokken, K.J. Mach, M.D. Mastrandrea, T.E. Bilir, M. Chatterjee, K.L. Ebi, Y.O. Estrada, R.C. Genova, B. Girma, E.S. Kissel, A.N. Levy, S. MacCracken, P.R. Mastrandrea, and L.L.White (eds.)], Cambridge, United Kingdom and New York, NY, USA, 1-32, 2014.

Jia, C., Tong, S., Zhang, W., Zhang, X., Li, W., Wang, Z., Wang, L., Liu, Z., Hu, B., and Zhao, P.: Pollution characteristics and potential sources of nitrous acid (HONO) in early autumn 2018 of Beijing, Science of The Total Environment, 735, 139317, 2020.

Jordan, C., Crawford, J. H., Beyersdorf, A. J., Eck, T. F., Halliday, H. S., Nault, B. A., Chang, L.-S., Park, J., Park, R., Lee, G., Kim, H., Ahn, J.-y., Cho, S., Shin, H. J., Lee, J. H., Jung, J.,

Kim, D.-S., Lee, M., Lee, T., Whitehill, A., Szykman, J., Schueneman, M. K., Campuzano-Jost, P., Jimenez, J. L., DiGangi, J. P., Diskin, G. S., Anderson, B. E., Moore, R. H., Ziemba, L. D., Fenn, M. A., Hair, J. W., Kuehn, R. E., Holz, R. E., Chen, G., Travis, K., Shook, M., Peterson, D. A., Lamb, K. D., and Schwarz, J. P.: Investigation of factors controlling PM2.5 variability across the South Korean Peninsula during KORUS-AQ, Elementa: Science of the Anthropocene, in review, 2020.

Joutsensaari, J., Ozon, M., Nieminen, T., Mikkonen, S., Lähivaara, T., Decesari, S., Facchini, M. C., Laaksonen, A., and Lehtinen, K. E.: Identification of new particle formation events with deep learning, Atmospheric Chemistry and Physics, 18, 9597-9615, 2018.

Kang, Y., Choi, H., Im, J., Park, S., Shin, M., Song, C.-K., and Kim, S.: Estimation of surface-level NO2 and O3 concentrations using TROPOMI data and machine learning over East Asia, Environmental Pollution, 288, 117711, 2021.

Kim, H., Gil, J., Lee, M., Jung, J., Whitehill, A., Szykman, J., Lee, G., Kim, D., Cho, S., Ahn, J., Hong, J., and Park, M.: Overview and characteristics of air quality in the Seoul Metropolitan Area during the KORUS-AQ campaign, Elementa: Science of the Anthropocene, in review, 2020.

Kleffmann, J., Lörzer, J., Wiesen, P., Kern, C., Trick, S., Volkamer, R., Rodenas, M., and Wirtz, K.: Intercomparison of the DOAS and LOPAP techniques for the detection of nitrous acid (HONO), Atmospheric Environment, 40, 3640-3652, 2006.

Kleinert, F., Leufen, L. H., and Schultz, M. G.: IntelliO3-ts v1. 0: a neural network approach to predict near-surface ozone concentrations in Germany, Geoscientific Model Development, 14, 1-25, 2021.

Krishnamurthy, R., Newsom, R. K., Berg, L. K., Xiao, H., Ma, P.-L., and Turner, D. D.: On the estimation of boundary layer heights: a machine learning approach, Atmospheric Measurement Techniques, 14, 4403-4424, 2021.

Lee, B. H., Wood, E. C., Zahniser, M. S., McManus, J. B., Nelson, D. D., Herndon, S. C., Santoni, G., Wofsy, S. C., and Munger, J. W.: Simultaneous measurements of atmospheric HONO and NO 2 via absorption spectroscopy using tunable mid-infrared continuous-wave quantum cascade lasers, Applied Physics B, 102, 417-423, 2011.

Levy, M., Zhang, R., Zheng, J., Zhang, A. L., Xu, W., Gomez-Hernandez, M., Wang, Y., and Olaguer, E.: Measurements of nitrous acid (HONO) using ion drift-chemical ionization mass spectrometry during the 2009 SHARP field campaign, Atmospheric Environment, 94, 231-240, 2014.

Li, S., Song, W., Zhan, H., Zhang, Y., Zhang, X., Li, W., Tong, S., Pei, C., Wang, Y., and Chen, Y.: Contribution of Vehicle Emission and NO2 Surface Conversion to Nitrous Acid (HONO) in Urban Environments: Implications from Tests in a Tunnel, Environmental Science & Technology, 55, 15616-15624, 2021a.

Li, Y., Wang, X., Wu, Z., Li, L., Wang, C., Li, H., Zhang, X., Zhang, Y., Li, J., and Gao, R.: Atmospheric nitrous acid (HONO) in an alternate process of haze pollution and ozone pollution in urban Beijing in summertime: Variations, sources and contribution to atmospheric photochemistry, Atmospheric Research, 260, 105689, 2021b.

Li, Z., Xie, P., Hu, R., Wang, D., Jin, H., Chen, H., Lin, C., and Liu, W.: Observations of N2O5 and NO3 at a suburban environment in Yangtze river delta in China: Estimating heterogeneous N2O5 uptake coefficients, Journal of Environmental Sciences, 2020.

Liebmann, J., Karu, E., Sobanski, N., Schuladen, J., Ehn, M., Schallhart, S., Quéléver, L., Hellen, H., Hakola, H., and Hoffmann, T.: Direct measurement of NO3 radical reactivity in a boreal forest, Atmospheric Chemistry and Physics, 2018.

Liu, Y., Lu, K., Li, X., Dong, H., Tan, Z., Wang, H., Zou, Q., Wu, Y., Zeng, L., and Hu, M.: A comprehensive model test of the HONO sources constrained to field measurements at rural North China Plain, Environmental science & technology, 53, 3517-3525, 2019.

Mallet, V., and Sportisse, B.: Uncertainty in a chemistry-transport model due to physical parameterizations and numerical approximations: An ensemble approach applied to ozone modeling, Journal of Geophysical Research: Atmospheres, 111, 2006.

Meng, F., Qin, M., Fang, W., Duan, J., Tang, K., Zhang, H., Shao, D., Liao, Z., Feng, Y., and Huang, Y.: Measurement of HONO flux using the aerodynamic gradient method over an agricultural field in the Huaihe River Basin, China, Journal of Environmental Sciences, 2022.

Monks, P. S., Archibald, A., Colette, A., Cooper, O., Coyle, M., Derwent, R., Fowler, D., Granier, C., Law, K. S., and Mills, G.: Tropospheric ozone and its precursors from the urban to the global scale from air quality to short-lived climate forcer, Atmospheric Chemistry and Physics, 15, 8889-8973, 2015.

Myhre, G., Aas, W., Cherian, R., Collins, W., Faluvegi, G., Flanner, M., Forster, P., Hodnebrog, Ø., Klimont, Z., and Lund, M. T.: Multi-model simulations of aerosol and ozone radiative forcing due to anthropogenic emission changes during the period 1990–2015, Atmospheric Chemistry and Physics, 17, 2709-2720, 2017.

Peterson, D. A., Hyer, E. J., Han, S.-O., Crawford, J. H., Park, R. J., Holz, R., Kuehn, R. E., Eloranta, E., Knote, C., and Jordan, C. E.: Meteorology influencing springtime air quality, pollution transport, and visibility in Korea, Elem Sci Anth, 7, 2019.

Pinto, J., Dibb, J., Lee, B., Rappenglück, B., Wood, E., Levy, M., Zhang, R. Y., Lefer, B., Ren, X. R., and Stutz, J.: Intercomparison of field measurements of nitrous acid (HONO) during the SHARP campaign, Journal of Geophysical Research: Atmospheres, 119, 5583-5601, 2014.

Reichstein, M., Camps-Valls, G., Stevens, B., Jung, M., Denzler, J., and Carvalhais, N.: Deep learning and process understanding for data-driven Earth system science, Nature, 566, 195-204, 2019.

Roberts, J. M., Veres, P., Warneke, C., Neuman, J., Washenfelder, R., Brown, S., Baasandorj, M., Burkholder, J., Burling, I., and Johnson, T. J.: Measurement of HONO, HNCO, and other inorganic acids by negative-ion proton-transfer chemical-ionization mass spectrometry (NI-PT-CIMS): Application to biomass burning emissions, Atmospheric Measurement Techniques, 3, 981, 2010.

Schultz, M., Betancourt, C., Gong, B., Kleinert, F., Langguth, M., Leufen, L., Mozaffari, A., and Stadtler, S.: Can deep learning beat numerical weather prediction?, Philosophical Transactions of the Royal Society A, 379, 20200097, 2021.

Shahriar, S. A., Kayes, I., Hasan, K., Salam, M. A., and Chowdhury, S.: Applicability of machine learning in modeling of atmospheric particle pollution in Bangladesh, Air Quality, Atmosphere & Health, 13, 1247-1256, 2020.

Shareef, M. M., Husain, T., and Alharbi, B.: Studying the Effect of Different Gas-Phase Chemical Kinetic Mechanisms on the Formation of Oxidants, Nitrogen Compounds and Ozone in Arid Regions, Journal of Environmental Protection, 10, 1006-1031, 2019.

Shindell, D. T., Lamarque, J.-F., Schulz, M., Flanner, M., Jiao, C., Chin, M., Young, P., Lee, Y. H., Rotstayn, L., and Mahowald, N.: Radiative forcing in the ACCMIP historical and future climate simulations, Atmospheric Chemistry and Physics, 13, 2939-2974, 2013.

Stadtler, S., Simpson, D., Schröder, S., Taraborrelli, D., Bott, A., and Schultz, M.: Ozone impacts of gas–aerosol uptake in global chemistry transport models, Atmospheric chemistry and physics, 18, 3147-3171, 2018.

Stevenson, D., Young, P., Naik, V., Lamarque, J.-F., Shindell, D. T., Voulgarakis, A., Skeie, R. B., Dalsoren, S. B., Myhre, G., and Berntsen, T. K.: Tropospheric ozone changes, radiative

forcing and attribution to emissions in the Atmospheric Chemistry and Climate Model Intercomparison Project (ACCMIP), Atmospheric Chemistry and Physics, 13, 3063-3085, 2013.

Sumathi, S., and Pugalendhi, G. K.: Cognition based spam mail text analysis using combined approach of deep neural network classifier and random forest, Journal of Ambient Intelligence and Humanized Computing, 12, 5721-5731, 2021.

Sun, Y., Wang, L., Wang, Y., Quan, L., and Zirui, L.: In situ measurements of SO2, NOx, NOy, and O3 in Beijing, China during August 2008, Science of the Total Environment, 409, 933-940, 2011.

Theys, N., Volkamer, R., Müller, J.-F., Zarzana, K. J., Kille, N., Clarisse, L., De Smedt, I., Lerot, C., Finkenzeller, H., and Hendrick, F.: Global nitrous acid emissions and levels of regional oxidants enhanced by wildfires, Nature geoscience, 13, 681-686, 2020.

Tie, X., Geng, F., Guenther, A., Cao, J., Greenberg, J., Zhang, R., Apel, E., Li, G., Weinheimer, A., and Chen, J.: Megacity impacts on regional ozone formation: observations and WRF-Chem modeling for the MIRAGE-Shanghai field campaign, Atmospheric Chemistry and Physics, 13, 5655-5669, 2013.

VandenBoer, T., Markovic, M., Sanders, J., Ren, X., Pusede, S., Browne, E., Cohen, R., Zhang, L., Thomas, J., and Brune, W. H.: Evidence for a nitrous acid (HONO) reservoir at the ground surface in Bakersfield, CA, during CalNex 2010, Journal of Geophysical Research: Atmospheres, 119, 9093-9106, 2014.

Varotsos, K., Giannakopoulos, C., and Tombrou, M.: Assessment of the Impacts of climate change on european ozone levels, Water, Air, & Soil Pollution, 224, 1-13, 2013.

Wang, H., Chen, X., Lu, K., Hu, R., Li, Z., Wang, H., Ma, X., Yang, X., Chen, S., and Dong, H.: NO3 and N2O5 chemistry at a suburban site during the EXPLORE-YRD campaign in 2018, Atmospheric Environment, 224, 117180, 2020.

Wang, T., Qin, Z., and Zhu, M.: An ELU network with total variation for image denoising, International Conference on Neural Information Processing, 2017a, 227-237.

Wang, X., Wang, H., Xue, L., Wang, T., Wang, L., Gu, R., Wang, W., Tham, Y. J., Wang, Z., and Yang, L.: Observations of N2O5 and ClNO2 at a polluted urban surface site in North China: High N2O5 uptake coefficients and low ClNO2 product yields, Atmospheric environment, 156, 125-134, 2017b.

Wolfe, G. M., Marvin, M. R., Roberts, S. J., Travis, K. R., and Liao, J.: The framework for 0-D atmospheric modeling (F0AM) v3. 1, Geoscientific Model Development, 9, 3309, 2016.

Xu, Z., Liu, Y., Nie, W., Sun, P., Chi, X., and Ding, A.: Evaluating the measurement interference of wet rotating-denuder–ion chromatography in measuring atmospheric HONO in a highly polluted area, Atmospheric Measurement Techniques, 12, 6737-6748, 2019.

Xue, C., Ye, C., Ma, Z., Liu, P., Zhang, Y., Zhang, C., Tang, K., Zhang, W., Zhao, X., and Wang, Y.: Development of stripping coil-ion chromatograph method and intercomparison with CEAS and LOPAP to measure atmospheric HONO, Science of The Total Environment, 646, 187-195, 2019.

Ye, C., Zhou, X., Pu, D., Stutz, J., Festa, J., Spolaor, M., Tsai, C., Cantrell, C., Mauldin, R. L., and Campos, T.: Rapid cycling of reactive nitrogen in the marine boundary layer, Nature, 532, 489-491, 2016.